



RESEARCH ARTICLE

10.1002/2016JA023738

Key Points:

- Diamagnetic depressions are found in the cusp and are observed to continue into the adjacent magnetosphere
- A heated plasma layer of mixed composition is found to depress the adjacent magnetospheric field
- Diamagnetic depression strength is correlated to solar wind dynamic pressure and velocity but not to the observed He⁺⁺ counts, like at Earth

Supporting Information:

- Supporting Information S1

Correspondence to:

J. M. Jasinski,
jjasinski@umich.edu

Citation:

Jasinski, J. M., C. S. Arridge, A. J. Coates, G. H. Jones, N. Sergis, M. F. Thomsen, and N. Krupp (2017), Diamagnetic depression observations at Saturn's magnetospheric cusp by the Cassini spacecraft, *J. Geophys. Res. Space Physics*, 122, 6283–6303, doi:10.1002/2016JA023738.

Received 25 NOV 2016

Accepted 3 MAY 2017

Accepted article online 11 MAY 2017

Published online 27 JUN 2017

©2017. The Authors.

This is an open access article under the terms of the Creative Commons Attribution License, which permits use, distribution and reproduction in any medium, provided the original work is properly cited.

Diamagnetic depression observations at Saturn's magnetospheric cusp by the Cassini spacecraft

Jamie M. Jasinski^{1,2,3} , Christopher S. Arridge⁴ , Andrew J. Coates^{2,3} , Geraint H. Jones^{2,3} , Nick Sergis^{5,6} , Michelle F. Thomsen⁷ , and Norbert Krupp⁸

¹Mullard Space Science Laboratory, University College London, London, UK, ²Centre for Planetary Sciences, University College London/Birkbeck, London, UK, ³Department of Climate and Space Sciences and Engineering, University of Michigan, Ann Arbor, Michigan, USA, ⁴Department of Physics, Lancaster University, Lancaster, UK, ⁵Office for Space Research and Technology, Academy of Athens, Athens, Greece, ⁶Institute of Astronomy, Astrophysics, Space Applications and Remote Sensing, National Observatory of Athens, Athens, Greece, ⁷Planetary Science Institute, Tucson, Arizona, USA, ⁸Max-Planck-Institut für Sonnensystemforschung, Göttingen, Germany

Abstract The magnetospheric cusp is a region where shocked solar wind plasma can enter a planetary magnetosphere, after magnetic reconnection has occurred at the dayside magnetopause or in the lobes. The dense plasma that enters the high-latitude magnetosphere creates diamagnetic effects whereby a depression is observed in the magnetic field. We present observations of the cusp events at Saturn's magnetosphere where these diamagnetic depressions are found. The data are subtracted from a magnetic field model, and the calculated magnetic pressure deficits are compared to the particle pressures. A high plasma pressure layer in the magnetosphere adjacent to the cusp is discovered to also depress the magnetic field, outside of the cusp. This layer is observed to contain energetic He⁺⁺ (up to ~100 keV) from the solar wind as well as heavy water group ions (W⁺) originating from the moon Enceladus. We also find a modest correlation of diamagnetic depression strength to solar wind dynamic pressure and velocity; however, unlike at Earth, there is no correlation found with He⁺⁺ counts.

1. Introduction

When magnetic reconnection occurs at the dayside magnetopause between the interplanetary magnetic field (IMF) and the closed magnetospheric field, the shocked solar wind plasma enters from the magnetosheath into the magnetosphere. The newly opened magnetospheric field line then convects poleward, and the injected plasma is observed in the cusp [e.g., Frank, 1971; Lockwood et al., 1994; Pitout et al., 2009]. Magnetic reconnection can also occur at the magnetopause in the magnetospheric lobes. The injected plasma displays various signatures, such as ion energy dispersions and depressions of the local magnetic field. This process and the associated cusp signatures have been observed at the Earth (see recent reviews by Smith and Lockwood [1996] and Cargill et al. [2005]), Mercury [e.g., Winslow et al., 2012; Raines et al., 2014], and Saturn [Jasinski et al., 2014, 2016a; Arridge et al., 2016].

The gyromotion of high-density magnetosheath plasma entering the magnetosphere can induce a diamagnetic depression observed as a decrease in the local magnetic field in the cusp [e.g., Erlandson et al., 1988; Niehof et al., 2008]. In previous reports at Earth, these depressions have been called “cusp diamagnetic cavities” (CDCs). CDCs have also been correlated to occur during energetic particle observations and have been named “cusp energetic particle” (CEP) events [Chen et al., 1997, 1998]. The authors reported the observation of high-energy He⁺⁺ in the cusp up to energies of 2 MeV, with the intensity peaking at 1–200 keV/q. The intensity of this range was also anticorrelated with the depth of the magnetic field depression in the cusp. The observation of these events has driven numerous studies to explain the origin of the diamagnetic events and the cusp energetic particles, and their relationship with each other.

This has led to three suggestions as to the origin of the CEPs: (1) local acceleration of ions in the cusp [e.g., Chen and Fritz, 1998; Fritz et al., 2003]; (2) acceleration at the bow shock [e.g., Trattner et al., 1999, 2001, 2003]; and (3) energization within the magnetosphere [e.g., Delcourt and Sauvaud, 1999; Asikainen and Mursula, 2005]. However, it has been shown that the turbulence interpreted to be ULF waves responsible for accelerating

the ions in the cusp [Chen and Fritz, 1998] is actually mostly caused by boundary motions over the spacecraft [Nykyri *et al.*, 2011a, 2011b]. It has also been demonstrated that energetic electrons cannot originate from the magnetosphere or the bow shock as they would not conserve the first adiabatic invariant [Nykyri *et al.*, 2012]. Nykyri *et al.* [2012] have suggested that particles can gain energies up to ~ 50 keV due to gradients in the reconnection "quasi-potential." However, the acceleration to MeV energies still needs to be further investigated [Trattner *et al.*, 2011].

A survey of observations from the Polar spacecraft [Zhou *et al.*, 2000] formed the basis of investigating the diamagnetic depressions in correlation to low-energy plasma with ion temperatures of ~ 100 eV. It has been found that the diamagnetic depressions are greater at (1) larger solar wind dynamic pressures at the magnetopause; (2) when the cusp is tilted toward the Sun, and (3) at local times closer to noon [Zhou *et al.*, 2001; Eastman *et al.*, 2000]. The depressions are also larger at larger radial distances from the planet, due to the rapid increase of geomagnetic field strength close to the planet [Tsyganenko and Russell, 1999; Lavraud *et al.*, 2004]. However, the differing spacecraft velocities at high altitudes ($\sim 10 R_E$) affect the observations; Clusters larger velocity (than Polar) results in a smoothing effect of the observed diamagnetic depression, and therefore, it is only measured during enhanced (>2 nPa) solar wind dynamic pressures [Nykyri *et al.*, 2011b]. Modeling by Adamson *et al.* [2011, 2012] showed that the location and size of the cusp diamagnetic depression is strongly dependent on the IMF orientation, and that it is mainly structured by reconnection processes.

Magnetic field depressions have also been observed at Mercury's cusp by the MErcury Surface, Space ENvironment, GEochemistry, and Ranging (MESSENGER) spacecraft [e.g., Winslow *et al.*, 2012; Raines *et al.*, 2014; Slavin *et al.*, 2014; Poh *et al.*, 2016], where the magnetic field is observed to be more turbulent and the depressions are larger in magnitude than at Earth. Poh *et al.* [2016] showed that the diamagnetic cavities are due to intense reconnection, with plasma flowing into the cusp in discrete flux tubes that had recently undergone reconnection.

Analysis of magnetospheric cusp observations at Saturn has been discussed in three previous papers. Jasinski *et al.* [2014] analyzed a single northern cusp traversal, where the ions displayed multiple "stepped" energy-latitude dispersion signatures which occurred due to reconnection occurring in "bursts" or "pulses" at various locations along the dayside magnetopause. Arridge *et al.* [2016] analyzed two southern cusp events and showed that the multiple cusp traversals observed were due to the cusp oscillating with the southern auroral oval (the southern auroral oval was shown to oscillate with a period of ~ 10.7 h by Nichols *et al.* [2008]).

Jasinski *et al.* [2016a] analyzed 11 days where the cusp was observed at Saturn. Eight of these cusps were analyzed for the first time, while three of these days had already been reported by Jasinski *et al.* [2014] and Arridge *et al.* [2016]. The cusps in these papers were identified due to either one or both of the following features typically observed at the cusp at Earth: (1) the presence of dense magnetosheath-like plasma displaying ion energy dispersions and (2) diamagnetic depressions. For more information about the plasma analysis and identification of these cusp events please see the references mentioned above. In this paper we focus on eight of these already identified Saturn cusp events specifically in regard to the diamagnetic depressions which were not analyzed in much detail (in the references mentioned above). The eight diamagnetic depression observations took place on the following days: 16 January 2007 (from now on referred to as "16JAN07"), 1 February 2007 ("1FEB07"), 8 March 2007 ("8MAR07"), 25 May 2008 ("25MAY08"), 21 January 2009 ("21JAN09"), 14 June 2013 ("14JUN13"), 24 July 2013 ("24JUL13"), and 17 August 2013 ("17AUG13"). The cusp was observed twice due to the oscillation of the auroral oval [Arridge *et al.*, 2016] for 16JAN07 and 1FEB07. To distinguish the two different diamagnetic depressions observed on these dates, we label them as 16JAN07-a, 16JAN07-b, 1FEB07-a, and 1FEB07-b. The double cusp observation of these two days results in 10 diamagnetic cusp observations. Except for one (8MAR07), all the cusp events occurred during dayside near-subsolar magnetopause reconnection. The 8MAR07 cusp occurred as a result of lobe reconnection [Jasinski *et al.*, 2016a]. All the cusp observations which occurred in the summer hemisphere presented a depression. The winter observations only present depressions in two out of five events (8MAR07 and 21JAN09). The other three cusp observations which were presented by Jasinski *et al.* [2016a] but are not analyzed here are 3 August 2008 ("3AUG08"), 24 September 2008 ("SEP08"), and 23 November 2008 ("NOV08"). These events did not present a diamagnetic depression and therefore are not discussed further.

In this paper the magnetic field observations in Saturn's cusp are investigated in more detail. The analysis involves comparing the magnetic field observations from the Cassini magnetometer (MAG) to that of a magnetic field model. The depth of the depressions is calculated as well as the consequent magnetic pressure

decreases. These results are compared to particle pressures observed by the plasma instruments. The association of energetic He^{++} solar wind ions with the diamagnetic depressions at Earth is well established [e.g., *Chen et al.*, 1997, 1998], and therefore, these particles at Saturn are also examined, as well as other high-energy particles that could be causing the depressions. First, we introduce the instrumentation, followed by the magnetic field model and the comparison to plasma pressure measurements.

2. Instrumentation and Observations

2.1. Instrumentation

The data presented in this paper is from instrumentation on board the Cassini spacecraft, including the magnetometer (MAG) [*Dougherty et al.*, 2004], the Cassini Plasma Spectrometer (CAPS) [*Young et al.*, 2004], and the Magnetospheric Imaging Instrument (MIMI) [*Krimigis et al.*, 2004].

One second averaged data are presented from MAG. CAPS is made up of three sensors, two of which are presented: the electron spectrometer (ELS) and the ion mass spectrometer (IMS). The energy range of ELS is 0.58–28,250 eV/q [*Linder et al.*, 1998; *Young et al.*, 2004]. The IMS observes positively charged ions with energies of 1–50,280 eV/q. The IMS also provides compositional information of the atomic and molecular ions, via a time-of-flight system (TOF). The information IMS can provide about the ions observed is produced as a function of energy per charge, direction of observation, and mass per charge (m/q). Therefore, IMS-TOF cannot distinguish ions with the same mass per charge, and therefore, it is not possible to differentiate between H_2^+ and He^{++} . In the magnetosphere, the $m/q=2$ population has been shown to most likely be H_2^+ [*Thomsen et al.*, 2010] originating from Titan [*Cui et al.*, 2008], largely found in the equatorial magnetodisk near the orbit of Titan. On the other hand, He^{++} is usually in the solar wind [*Thomsen et al.*, 2010; *Arridge et al.*, 2016]. Therefore, we assume that in the cusp the $m/q=2$ ions observed by IMS are of He^{++} . Another main source of ions from within the Saturnian system is from the moon Enceladus, which produces heavy water group ions such as O^+ , OH^+ , H_2O^+ , H_3O^+ , and O_2^+ (collectively called “ W^+ ”).

The sensor used on MIMI is the charge energy mass spectrometer (CHEMS), which is similar to IMS in that it uses electrostatic analysers and carbon foils followed by TOF to identify the composition of ions [*Krimigis et al.*, 2004]. The energy per charge range of the instrument is 3–220 keV/q. The detector can determine the mass per charge, mass, charge, and energy of the ions. This is an important distinction from IMS-TOF, which only gives mass per charge. This means that CHEMS can, for example, distinguish between He^{++} and H_2^+ , while IMS is unable to do so.

2.2. Example of a Cusp Observation

An example of a Cassini trajectory through the cusp is shown in Figure 1 for the 1FEB07-a and 1FEB07-b events (red bar). The data from the period in between the green bars is shown in Figures 1a–1c. The spacecraft is traveling equatorward, and the data begin with Cassini traversing field lines connected to the polar cap. Cassini then crosses through the cusp where dense magnetosheath-like plasma is observed, followed by traversing the magnetosphere (higher-energy and less dense than the cusp) before observing the cusp a second time. The cusp observations display ion energy-latitude dispersions characteristic of the terrestrial cusp. Diamagnetic depressions are also observed. The spacecraft reenters the magnetosphere before crossing the magnetopause four times and observing the magnetosheath twice. This particular observation occurs under significant magnetospheric compression by the solar wind as the average magnetopause standoff location is $\sim 22\text{--}27 R_S$ [*Achilleos et al.*, 2008], while the magnetopause is crossed here at $16.5 R_S$. The plasma analysis of this particular cusp event is the focus of a previous paper [*Arridge et al.*, 2016]. At the end of this data set a flux transfer event is observed (twisted magnetic fields in a rope-like configuration which occur due to multiple reconnection) which was analyzed and discussed by *Jasinski et al.* [2016b].

3. The Magnetic Field Model

The data were compared to a magnetic field model in order to calculate the magnetic pressure change during the depression. The position of the spacecraft was used to define the location in the model magnetic field. At this location the model then calculated the strength of an axisymmetric, internal magnetic field (therefore B_ϕ was not in this model) with superimposed model ring current fields. The axisymmetric internal magnetic field was calculated as a spherical harmonic expansion and used the coefficients from *Burton et al.* [2010] (g_1^0 , g_2^0 , and g_3^0 are the Gauss coefficients—dipole, quadrupole, and octupole—taken to be 21,191 nT, 1586 nT, and 2374 nT, respectively).

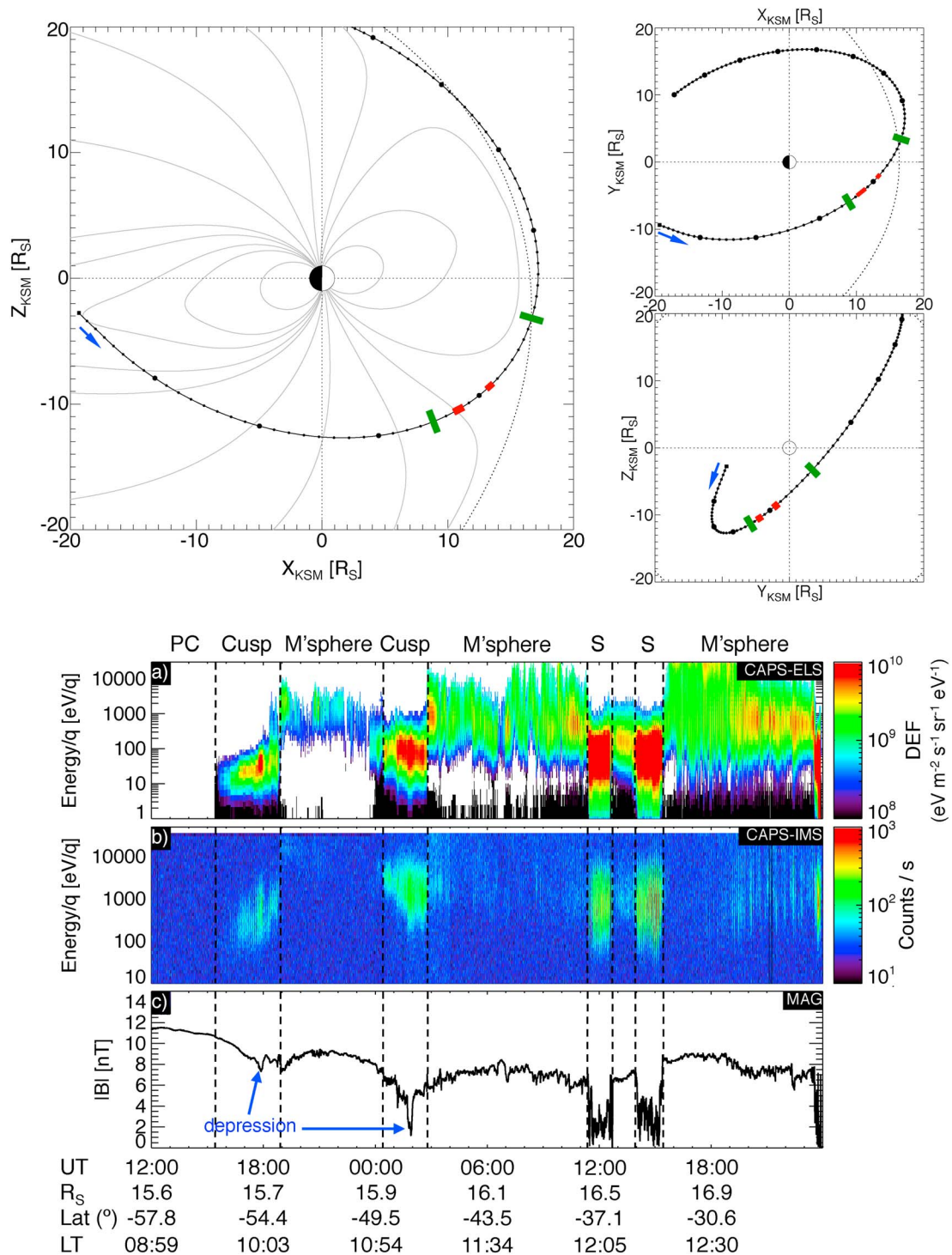


Figure 1. An example of a Cassini trajectory between 29 January and 10 February 2007. At the top (clockwise) we have the trajectory in the Kronocentric Solar Magnetospheric (KSM) coordinate system, in the X-Z plane (“view” from dawn), X-Y plane (looking down onto the equatorial plane with the equatorial plane inclined out of the page on the dayside), and the Y-Z plane (view from the Sun). Large dots signify the start/end of days, while the smaller dots represent 3 h intervals in UTC. This trajectory figure is reproduced and adapted from *Jasinski et al. [2016b]*. The blue arrow represents the direction of Cassini. The red bars show where the cusp was observed for the 1FEB07-a and 1FEB07-b events. The green bars indicate the extent of the data shown in (a) omnidirectional low-energy electron flux from CAPS-ELS, (b) ions from IMS, and (c) the magnetic field measurements from MAG. “PC,” “S,” and “DEF” stand for polar cap, magnetosheath, and differential energy flux, respectively. The cusp plasma analysis during this interval is discussed in detail by *Arridge et al. [2016]*.

The model also generates magnetic fields induced by the ring current. The ring current parameters were taken from *Bunce et al.* [2007]. These parameters were dependent on the subsolar positions of the magnetopause, which are predicted using velocity and density propagations by the Michigan Solar Wind Model (mSWiM) to calculate the standoff distance. mSWiM is a model that propagates solar wind conditions from observations at 1 AU, outward [Zieger and Hansen, 2008]. mSWiM is most accurate for propagations within 75 days of opposition [Zieger and Hansen, 2008]. All of the events analyzed here occurred within 75 days of apparent opposition. The field vectors associated with the ring current sheet were calculated from the model described by *Connerney et al.* [1981, 1983], using the analytical approximations presented in *Giampieri and Dougherty* [2004]. The cylindrical radial and axial components of the model field were then transformed to radial and theta components (B_r and B_θ) in Kronographic-Radial-Theta-Phi coordinates. These values were then added to the axisymmetric field vectors from the internal model. A small error is introduced in using the *Connerney et al.* [1981, 1983] model because it has been shown that at Saturn, the radial profile of the ring current is not the same (i.e., a $1/r$ drop off) such as the one the model adopts [Sergis et al., 2010]. *Sergis et al.* [2017] report that the azimuthal current density uncertainty can only be roughly estimated and use a liberal $\sim 50\%$ error on the density. *Kellett et al.* [2010] find that despite this, the model does reproduce the gross features of the current density profile. With all this in mind we do not expect our results here to be affected significantly anyway.

After calculating the model magnetic field at the position of the spacecraft, the method described further below was used to calculate the magnetic pressure deficit associated with the decrease in the observed magnetic field data from MAG. The calculated magnetic pressure deficits were then compared to the observed plasma pressure to investigate any anticorrelation. This method has been previously used to compare the magnetic and plasma pressures at Mercury's equatorial magnetosphere [Korth et al., 2011], as well as the cusp at Mercury [Winslow et al., 2012], both of which used data from the MESSENGER spacecraft.

By comparing the MAG data to the magnetic field model, the depression was selected by eye from where the MAG data (observed magnitude) first departed from the general trend of the model. This can be seen in an example (for the JUN13 event) in Figure 2a. The observed magnetic field (MAG; black) at 19:40 UT is no longer decreasing at the same rate as the field model (shown in red), which is taken to be the start of the depression. The observed field is at a minimum at $\sim 21:00$ UT, which marks the center of the depression. At 22:20 UT, the observed field resumes its general decrease in magnitude similar to the field model.

The model magnetic field was subtracted from the observations, to obtain the total residual field $B_{res} = |B|_{obs} - |B|_{model}$. The result of this subtraction (B_{res}) can be seen in Figure 2b, where the black residual field highlights the depression and the red shows the constant residual field. The background unperturbed residual magnetic field was calculated during the depression by applying a third degree polynomial fit (blue) to the residual field (i.e., before and after the depression) shown in red. The polynomial fit represents the residual field in the absence of a diamagnetic depression.

The calculated polynomial fit was then added to the model, so that the unperturbed magnetic field could be estimated. B_{res} was then subtracted from the unperturbed field and the result was used to calculate the magnetic pressure (p_B) using the magnetic pressure equation: $p_B = B^2/2\mu_0$, where B is the magnetic field magnitude and μ_0 is the permeability of free space. This pressure thus represents the magnetic pressure deficit that occurs due to the depression. This calculation can be written in the following equation:

$$\Delta p_B = \frac{(|B_{model} + \Delta B_m|^2 - |B|^2)}{2\mu_0} \quad (1)$$

where ΔB_m is the polynomial fit and Δp_B is the magnetic pressure deficit arising from the observed depression. The resulting pressure deficit resulting from the magnetic depression can be seen in Figure 2c.

This pressure deficit is used to predict the plasma pressure increase that is required to balance the total plasma pressure considering this is a diamagnetic effect, from $P_{Plasma} = P_{Total} - P_{Mag}$. This calculated pressure will be compared to the observed particle pressures.

This method was applied to all the observed diamagnetic depressions. A summary of the magnetic pressure deficits of all the cusp observations (in comparison) can be seen in Figure 3. Figures 2c and 3h are the same. The panels are arranged chronologically. The time is centered on the center of the depressions characterized as 00:00 (hh:mm), so that the duration of the observations can be compared. The pressures are on the same scale so that the depth of the depressions can also be compared. The dashed lines indicate the entry and exit

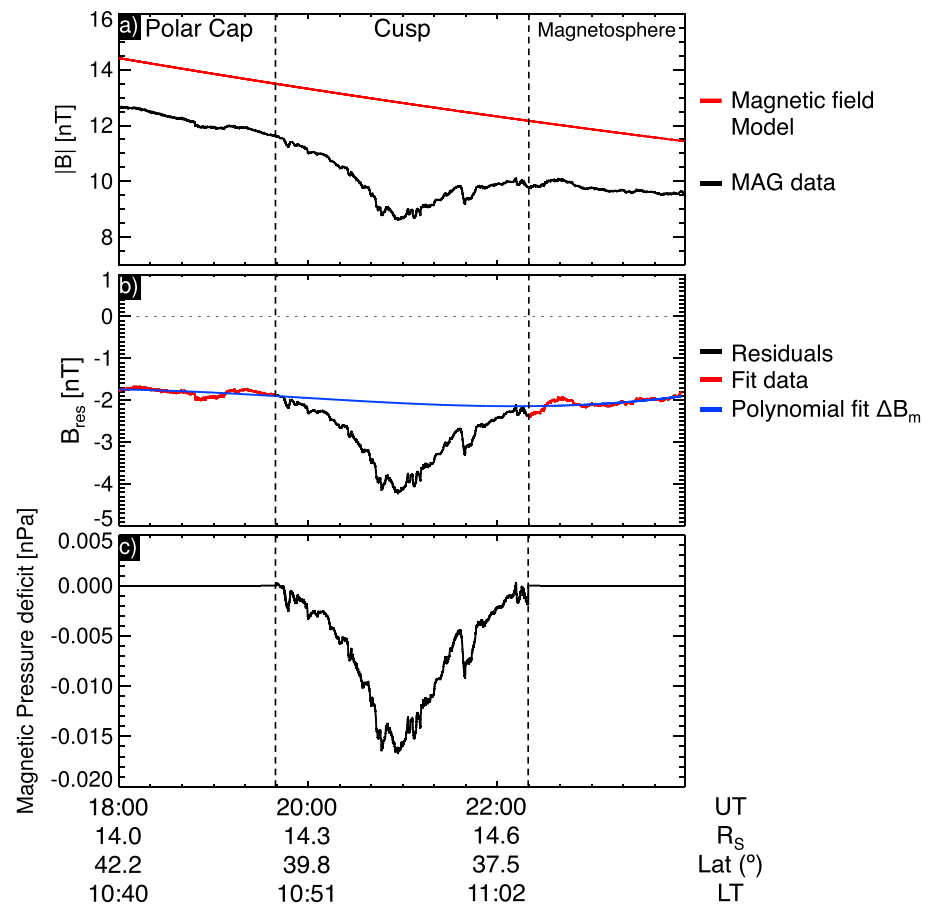


Figure 2. An example of the magnetic model, MAG data, and the pressure calculated for the 14JUN13 cusp. (a) The model (red) and 1 second average MAG data, (b) the residuals of the magnetic depression (black) the fitted residual before and after the depression (blue) and the polynomial fit (red), and (c) the calculated magnetic pressure deficit.

of the cusp intervals as categorized by CAPS observations in previous papers [Arridge *et al.*, 2016; Jasinski *et al.*, 2014]. Figures 3a–3e are observations of the southern cusp (summer), Figures 3f and 3g are of the northern cusp (winter), and Figures 3h–3j are of the northern cusp (summer). Figure 3f shows the two entries and exits of the cusp observations for the 25MAY08 event (as described in Jasinski *et al.* [2016a]), which were separated by a boundary layer.

It should be noted that the last major depression during the 25MAY08 (Figure 3f) observation at $\sim +02 : 00$ is most likely an artifact of the magnetic field model subtraction due to such large magnetic field strengths as well as an uncharacteristically varying background magnetospheric field. However, the first two decreases in pressure are observed in the magnetic field data as diamagnetic depressions (specifically the depressions at approximately $-03:00$ and $-00:30$), which display the characteristic magnetic field variability of magnetosheath-like plasma. The 25MAY08 observation has the most dramatic and the strongest magnetic pressure decrease (please see supporting information Figure S3 for more details). This is due to the field strengths being significantly higher, with total field magnitudes of ~ 30 to 40 nT, which produce larger Δp_B in equation (1). In comparison the field strengths in the other depressions occur between ~ 8 and 15 nT. The JAN07-b depression has the second strongest magnetic pressure decrease, due to the field being depressed to a magnitude of ~ 2 nT ($\sim 85\%$ magnetic field magnitude decrease). The regions on either side of the cusp (for 16JAN07-b) can clearly be seen to also depress the magnetic field. The entrance into the depression starting in the magnetosphere followed by start of the cusp forms a shallow depression, and then Cassini observes large variability in the depression where there are severe decreases of the magnetic field. Another two depressions are observed upon exiting the cusp, in the magnetosphere again.

Magnetic depression observations in 2007 (Figures 3a–3e) and the final observation (Figure 3j) can be seen to not be at the center of the cusp interval (as indicated by the dashed lines), and instead continue into

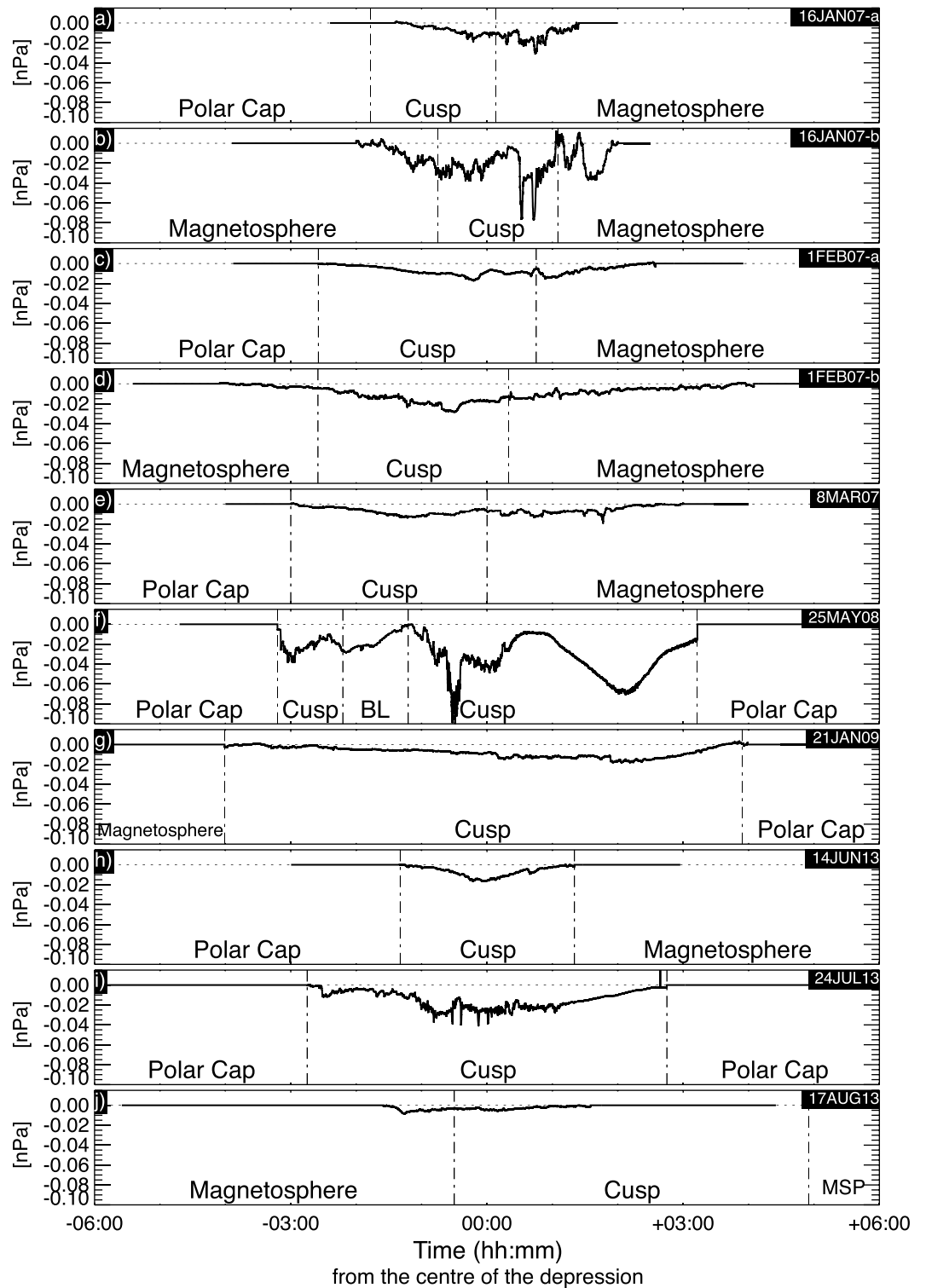


Figure 3. The magnetic pressure deficits of all the cusp observations listed chronologically with the 16JAN07 and 1FEB07 separated into their two separate cusps *a* and *b*. The *x* axis is zero on the center time of the depressions, and time is displayed in the hh:mm format, with 6 h on either side of the center. The dashed lines represent the entry and exit of cusp plasma interval as characterized by CAPS observations described in previous papers [Jasinski et al., 2014, 2016a; Arridge et al., 2016].

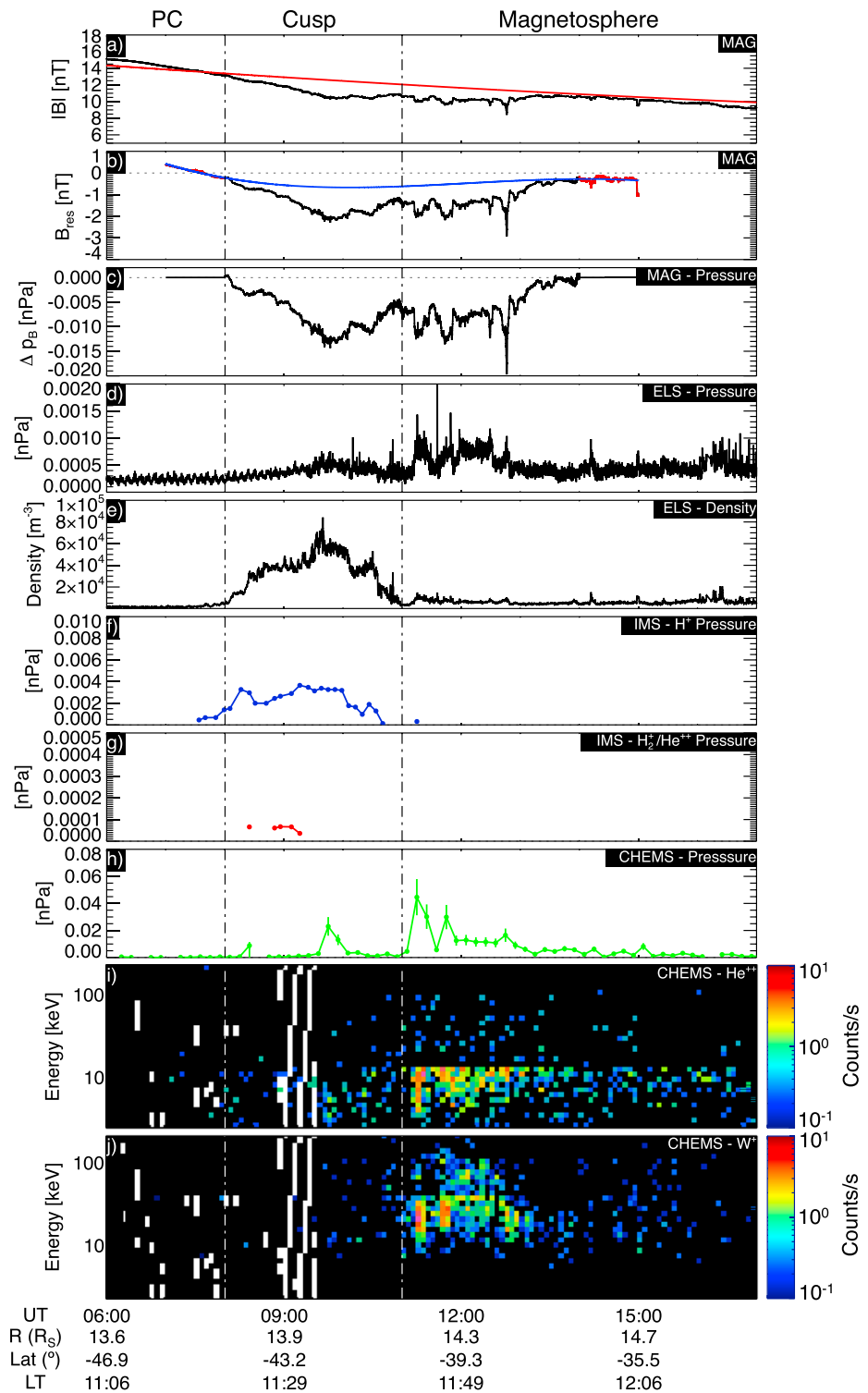


Figure 4. All the pressure observations for the 8MAR07 event, including (a–c) magnetic pressure analysis (in the same format as Figure 2). Also shown are particle pressure measurements from various instrumentation: (d and e) electron pressure and density, respectively, from ELS; (f and g) proton and $m/q = 2$ pressure, respectively, from IMS; (h) CHEMS energetic particle pressure; and (i and j) time-energy spectrograms for He^{++} and W^+ observed by CHEMS are also shown. The pressure axes are not uniformly scaled.

the magnetosphere. For the 16JAN07-b event, the depression occurs on either side of the cusp (i.e., in the magnetosphere). The Saturn magnetic pressure depressions (associated with the cusp intervals) will now be compared to plasma pressure observations from various in situ instruments onboard Cassini.

4. Comparison of Plasma and Magnetic Pressures

4.1. Overview for 8MAR07

The magnetic field analysis and pressure deficit calculation as well as the particle pressure components for the 8MAR07 depression are presented in Figure 4. Figures 4a–4c are in the same format as Figure 2. Figures 4 show calculated CAPS moments including (d) ELS pressure, (e) ELS density, (f) IMS proton pressure, and (g) IMS $m/q = 2$ pressure (what we assume to be He^{++} as mentioned in the instrumentation section). Figure 4h shows the calculated high-energy particle pressure from CHEMS. The CHEMS He^{++} and W^+ observations are also shown in Figures 4i and 4j, as time-energy spectrograms. The vertical dashed lines show where the cusp is during these observations (the first half of the depression). The pressures are not scaled, so that each component can be fully seen. The magnetic pressure deficit (Figure 4c) reaches a general trough of -0.012 nPa in and outside the cusp.

Much of the electron pressure (Figure 4d) is at the noise level (~ 0.25 nPa), except for the latter half of the cusp and the second half of the depression. The electron pressure contributes the least to the total plasma pressure due to the very small electron mass; however, the depression changes in the cusp are directly anticorrelated to the electron density. Figure 4e shows that the depression is a diamagnetic effect.

The energetic particle pressure (from CHEMS) is the most dominant component of the plasma pressure. The peaks are anticorrelated with the magnetic pressure deficit troughs. The CHEMS pressure peaks are higher (~ 0.025 and ~ 0.045 nPa) than the magnitude of the magnetic pressure deficits (~ 0.012 nPa).

During the latter half of the depression (adjacent to the cusp, in the labeled “magnetosphere”) there is an increase in flux of both energetic He^{++} and W^+ ions (Figures 4i and 4j). Increased counts of both (with high energies) show this region to be a heated, mixed plasma. We assume that the alpha particles are of a solar wind origin.

Water group ions are of a magnetospheric origin; however, [Sergis *et al.*, 2013] found that the magnetosheath has a presence of hot (keV) W^+ ions that escape the magnetosphere due to large gyroradii effects. Therefore, it is not possible to tell whether both of these species originate from the magnetosheath, or whether the observed W^+ is directly observed from the magnetosphere. It is interesting that the hot W^+ is adjacent to the cusp and not in the cusp with the magnetosheath plasma, since one would expect to observe both simultaneously. For this reason we assume that the plasma in the cusp and the heated layer in the magnetosphere do not share a common origin.

At Earth, the cusp magnetic depressions are usually centered on the high-density magnetosheath-like plasma. In the 8MAR07 example, the depression is observed to continue into the magnetosphere where there is evidently a high-pressure, mixed plasma layer next to the cusp, characterized by the (energetic) high CHEMS pressures and increased counts of He^{++} and W^+ . This is a different region to the “boundary layer” that is discussed by Arridge *et al.* [2016] and Jasinski *et al.* [2016a]. The boundary layer was observed as a gradual increase of energy (and decrease in flux) of electrons observed in ELS. An example of this can be seen in Figure 5, labeled BL. The transition can be seen between the low-energy magnetosheath-like plasma in the cusp and the higher-energy tenuous plasma in the magnetosphere. However, once the spacecraft is in the higher-energy region—labeled “depressed m’sphere layer”—the magnetic field depression continues until the particle count of He^{++} and W^+ in CHEMS and electron flux in ELS both decrease significantly.

The resolution for MAG at a dynamic range of ± 40 nT for MAG is 4.9 pT [Dougherty *et al.*, 2004]. The uncertainty on the CHEMS pressure is dependent on the count rate during the interval. The data have a time resolution of 10 min, and so the uncertainty will be the square root of the total counts during this time interval. For a resolution of 10 min the uncertainty will be 4%–13% (for a count rate of 1 c/s–0.1 c/s) [Sergis *et al.*, 2009]. An additional error of less than 30% is present due to CHEMS underresolving the pitch angle distribution which is lower than the scatter in the data due to the dynamics of the system. This is the general understanding of the CHEMS pressure calculations but is not run for each pressure moment.

Arridge *et al.* [2009] estimate the errors for the density and temperature for the CAPS-ELS data, and for values found in the cusp the error is of the order of 10% or less (for both the density and temperature). The technique

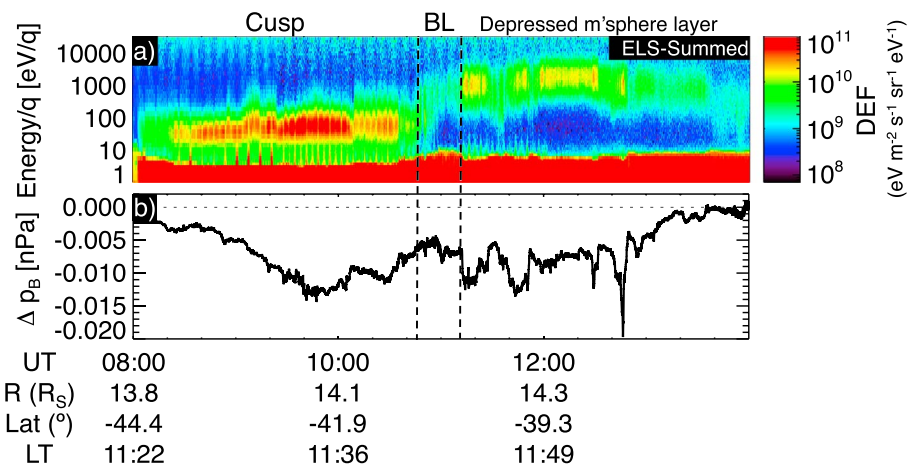


Figure 5. ELS observations (a) of the different layers adjacent to the cusp, with the (b) magnetic pressure deficit for the 8MAR07 cusp. The boundary layer “BL” has been discussed in the text. The high-pressure magnetospheric layer which continues the depression of the magnetic field outside the cusp is also labeled.

run by *Arridge et al.* [2009] is an analysis of the noise properties of CAPS-ELS and their effect on the plasma moments, and as such does not provide an estimate of uncertainty for every plasma moment.

4.2. Summary of 16JAN07 and 1FEB07

The 16JAN07-a and 16JAN07-b and 1FEB07-a and 1FEB07-b (Figures 6 and 7, respectively) magnetic field analyses as well as the plasma pressure observations are presented in the same format as for the 8MAR07 overview shown in Figure 4.

The 16JAN07-a depression peaks in the magnetosphere ($\sim 12:30$ UT), and the observation of the cusp only makes the depression appear more gradual when traversing from the polar cap to the magnetosphere. This morphology of the magnetic depression is the same as the MAR07 event, where the depression is also observed in the magnetosphere. The electron pressure is very low in the cusp due to the low energies, with an increase in the magnetosphere (higher energies), where it is anticorrelated to the magnetic pressure decrease. The depression begins when there is large increase in the electron density (when the spacecraft is partway through the cusp). Similar behavior has been reported at Earth, where a magnetic decrease coincides with an increase in density within the cusp, causing the depression to not always persist throughout the whole cusp crossing [*Niehof et al.*, 2008]. The IMS H^+ pressure steadily increases and maximizes during the minimum depression and accounts for approximately half of the magnetic pressure decrease. The high-energy ion pressure in CHEMS contributes the other half of the pressure equivalent to the depression, also peaking in the magnetosphere.

The start of the depression in the 16JAN07-b event occurs (at $\sim 15:30$ UT) with a large increase in the $m/q = 2$ ion pressure (IMS), but it is still lower than the other pressure components. The cusp region (the start of which is marked by the third dashed line in Figure 6) occurs during extremely large increases of pressure observed by CHEMS (increase from 0.1 nPa to 0.5 nPa) with a large increase in flux observed of energetic W^+ ions by CHEMS. However this pressure enhancement is significantly larger than the magnitude of the magnetic pressure decrease (0.02 nPa). During the JAN07-b depressions, the CHEMS pressure does not follow an anticorrelated trend to the magnetic pressure deficit. The first depression is shallow but has a large CHEMS pressure increase, while the following deep depression sees a decrease in the CHEMS pressure at $\sim 17:30$ UT.

From $\sim 17:30$ UT, increases in He^{++} and H^+ pressures are observed (~ 0.006 nPa and ~ 0.04 nPa, respectively) as well as a significant increase in the electron density and pressure. The ion data are at too low a time resolution to be able to determine whether there is an increase in pressure during the two strongest depressions in the magnetic field. The final two small depressions in the magnetosphere occur during increases in flux of energetic He^{++} and W^+ (CHEMS) as well as an observed increase in the ELS pressure.

Figure 7 presents pressure observations for the 1FEB07-a and 1FEB07-b events. The minimum magnetic pressure depression inside the 1FEB07-a cusp (at $\sim 17:50$ UT) occurs during significant increases of all the components of the plasma pressure (except for electrons), including a burst of pressure observed in CHEMS.

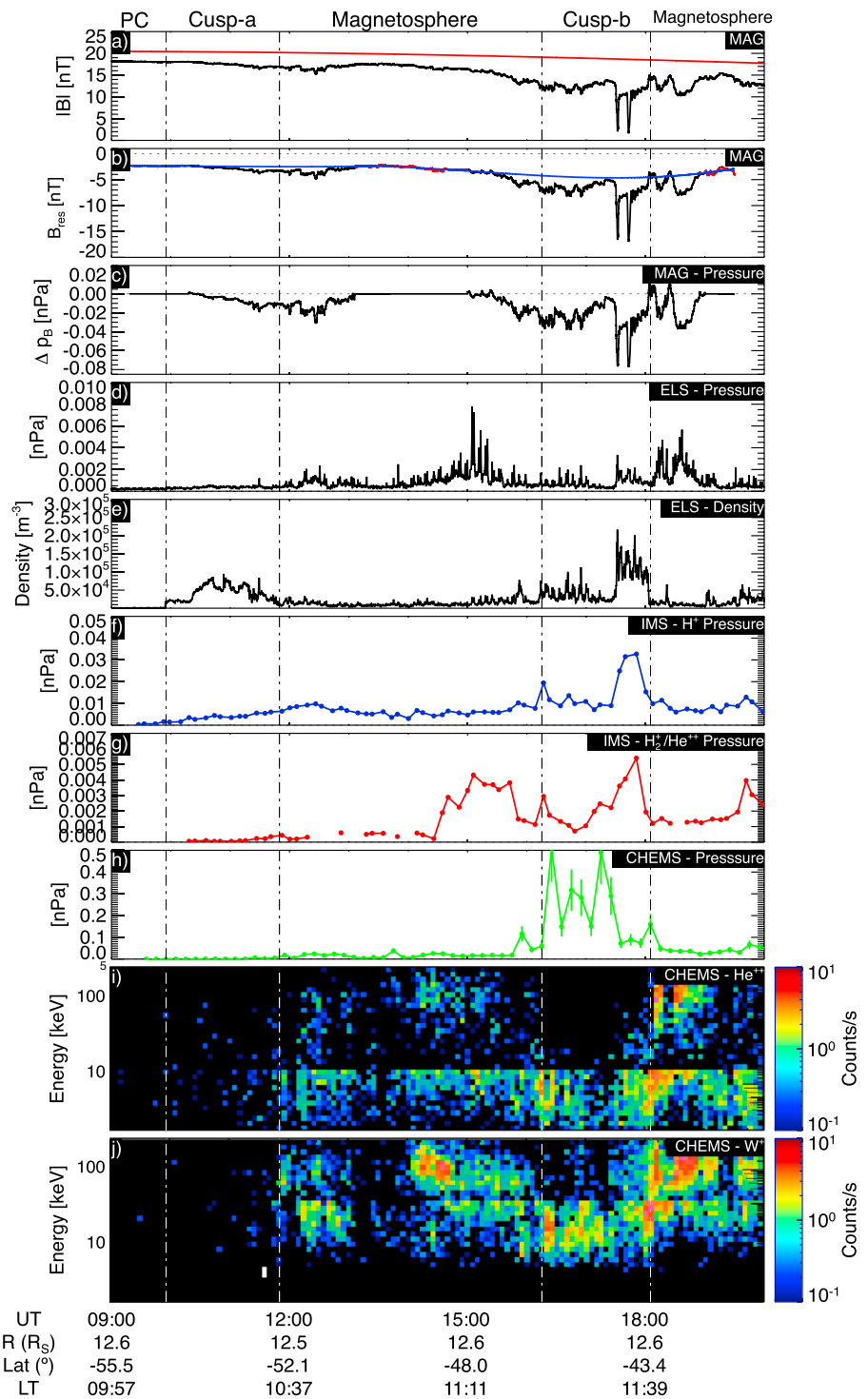


Figure 6. All the particle pressure observations, including the (a–c) magnetic pressure analysis for the 16JAN07-a and 16JAN07-b events. This figure is in the same format as Figure 4.

Similar to the 8MAR07 event, the depression is seen with a large increase in electron density. Similarly to the 8MAR07 event, the depression continues into the magnetosphere, and it is during this interval that an increase in flux can be seen in the energetic He⁺⁺ and W⁺ (Figures 7i and 7j) as well as an increased electron pressure.

The second depression is observed (between the third and fourth dashed lines) during a burst of energetic He⁺⁺ at the 1 keV energy level, as well as increased electron and energetic ion pressures. A burst of W⁺ is

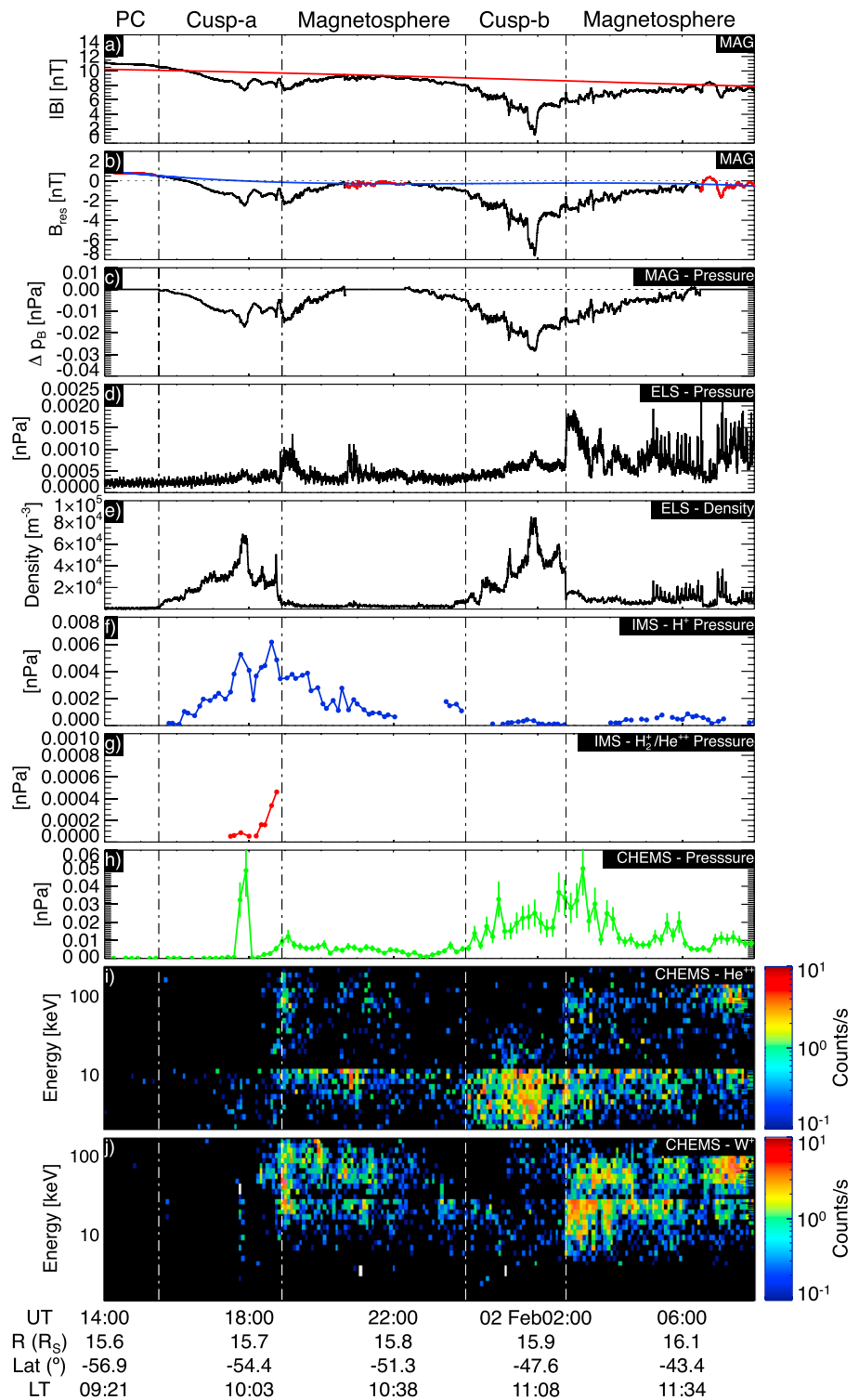


Figure 7. All the observations pressure observations, including the (a–c) magnetic pressure analysis for the 1FEB07-a and 1FEB07-b event. This figure is in the same format as Figure 4.

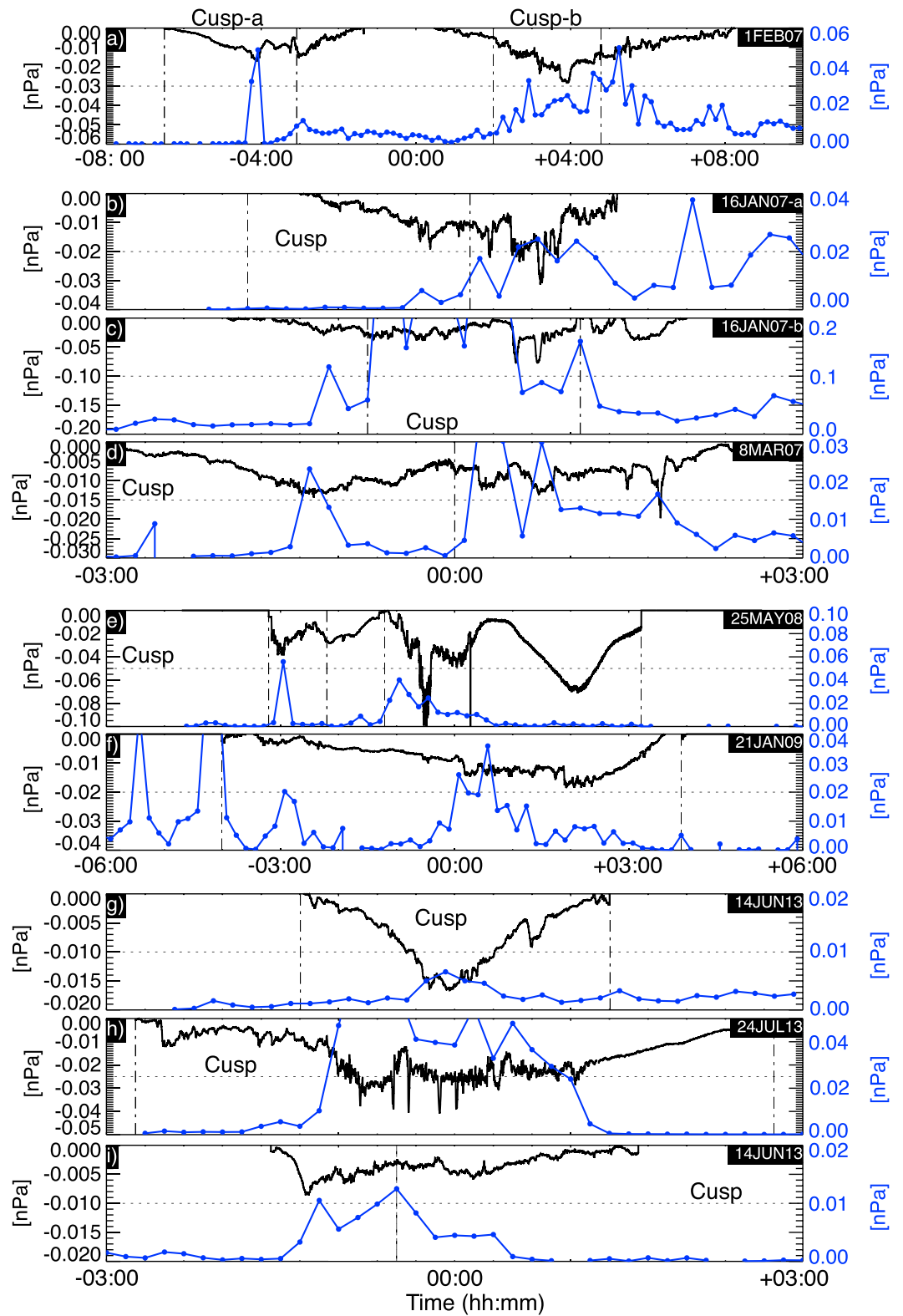


Figure 8. A summary of all the magnetic pressure deficit estimates (black) and their comparison to the CHEMS pressure (blue). Both pressures are shown on the same scale with a horizontal dotted line shown at the midpoint.

observed upon exiting the cusp at the end of the depression, including high electron pressures. The magnetic pressure deficit in the first cusp is ~ 0.015 nPa, while the pressures increase by ~ 0.05 and 0.005 nPa (CHEMS and IMS). In the second cusp the pressure changes are more similar at ~ 0.03 nPa. In the first cusp encounter, there is a discrepancy between the observed plasma and magnetic pressure changes, with the plasma pressure significantly larger. Upon exiting the second cusp, the magnetic depression does not end but continues to decrease in magnitude gradually during a coincident decrease in CHEMS pressure. During this period, even though the plasma pressure is decreasing, it remains larger than the magnitude of the magnetic pressure deficit.

4.3. Summary of Other Observations

These observations are all presented separately in separate figures in the supporting information (in the same format as Figures 4, 6, and 7).

A summary of the magnetic pressure deficit and the CHEMS pressure (the most dominant plasma pressure in the cusp) for each of the cusp event is shown in Figure 8. This figure shows that there is rarely a balance between the two pressures. However, we do see that the changes in pressures are usually well anticorrelated, with dramatic increases in plasma pressure occurring during decreases of magnetic pressure, even if the change in one is not equal to the change in the other.

For the 25MAY08 observation the magnetic depression is well correlated with the electron pressure and density; however, the plasma pressure increase of all the components at $-00:30$ (Figure 3f) does not account for the total magnetic pressure change, which is the largest observed at ~ 0.1 nPa. Even though there are large peaks in all of the low-energy plasma pressure components, the plasma pressure change is much lower than that in the magnetic pressure, in contrast to previous examples. There is also a large increase in flux observed in the energetic He^{++} ions during this central depression trough.

H^+ (IMS) pressure during the 21JAN09 event is the most anticorrelated to the magnetic depression. There do seem to be increases in the CHEMS pressure which correlate to significant decreases in the magnetic field, where the pressure of the magnetic depression is higher than the CHEMS pressure.

The final observed magnetic depressions occurring in 2013 are all very well correlated with increases in CHEMS pressures. For 14JUN13 the observed plasma pressure, however, is less than half the value of the magnetic pressure decrease. For the JUL13 and AUG13 events the CHEMS pressures overcompensate for the magnetic pressure decrease by ~ 0.06 nPa and up to ~ 0.006 nPa, respectively. There is also a very large increase in the energetic He^{++} flux (the highest fluxes observed in the cusp) for the 24JUL13 event, as well as some increase in energetic water group ion flux. This indicates that this plasma is composed of mixed solar wind and magnetosphere particles. The 17AUG13 depression is mainly centered on the high W^+ fluxes in the magnetosphere, with the depression decreasing in the cusp (similar to the southern observations: 8MAR07, 16JAN07-a, 1FEB07-a, and 1FEB07-b).

5. Latitudinal and Solar Wind Effect Correlations

Figure 9 shows the magnetic depression relationship with the dynamic pressure and velocity of the solar wind (using the mSWiM solar wind propagations from 1 AU to 9 AU). The error bars shown represent the ~ 15 h temporal uncertainty associated with the mSWiM model [Zieger and Hansen, 2008]. The Pearson correlation coefficient (r) which gives a measure of how well parameters are correlated has also been calculated. The Pearson coefficient is equal to 1 for a perfect positive correlation, -1 for a perfect anticorrelation, and 0 when no correlation is present. A strong positive correlation was found for the solar wind dynamic pressure, and a moderate positive correlation for the velocity.

These figures indicate that the depression is generally greater for larger solar wind dynamic pressures and velocities. A compressed magnetosphere and high solar wind velocities have been found to produce larger reconnection voltages at the magnetopause [Jackman *et al.*, 2004]. This has also been reported [Zhou *et al.*, 2001] at the terrestrial magnetosphere (where diamagnetic depression depth increased with solar wind dynamic pressure).

No correlations could be found with the Alfvénic Mach number (MA) of the solar wind and the depressions. As mentioned previously, one would expect larger depressions in the cusp to occur with higher upstream MA values, as this would be associated with a stronger shock, a more dense magnetosheath and therefore larger

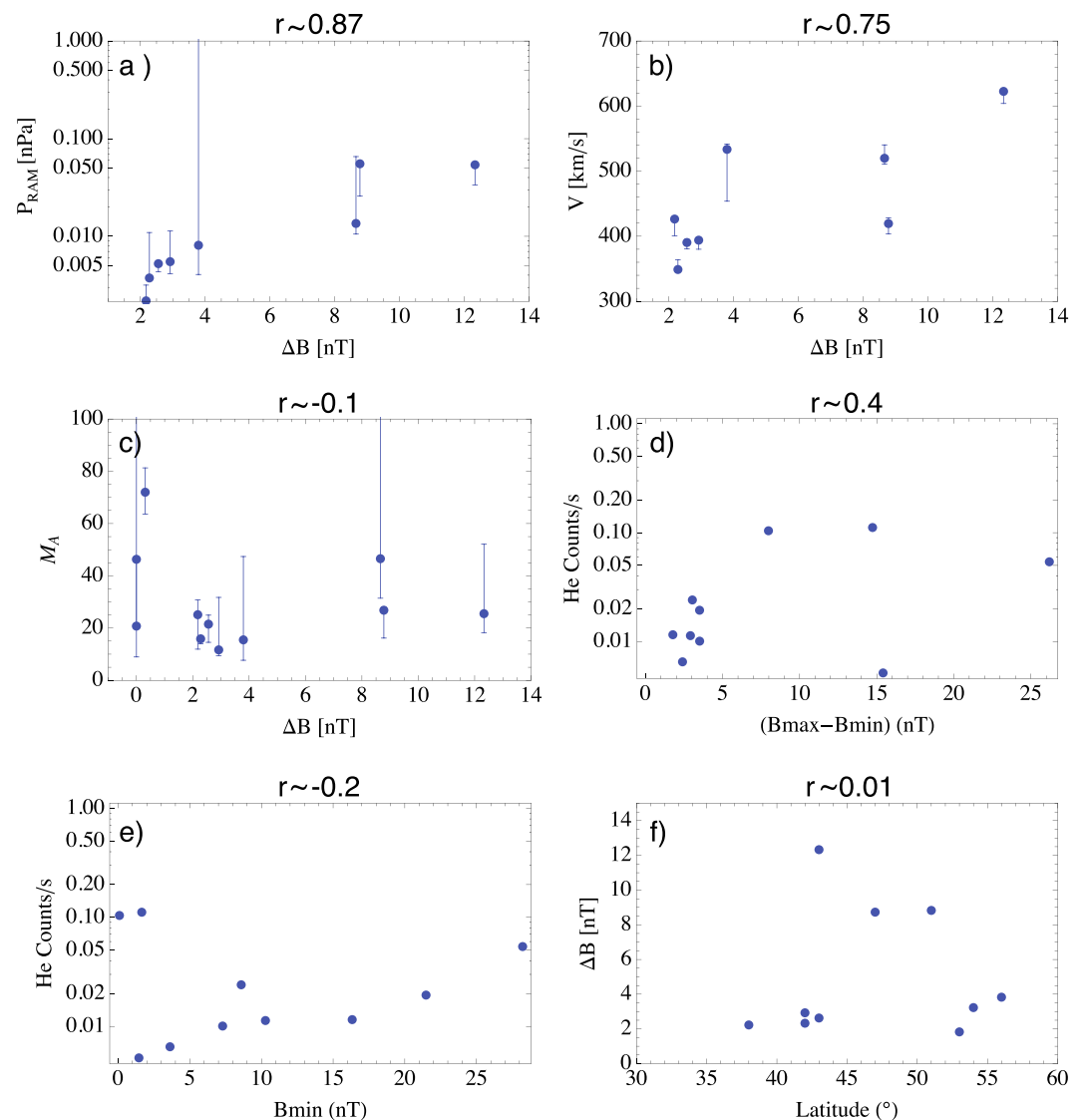


Figure 9. The correlations between the depth of the magnetic field measurements (ΔB) in the cusp and the solar wind parameters: (a) dynamic pressure P_{RAM} , (b) velocity, and (c) Alfvénic Mach number (M_A). Also shown are the correlations to the helium observations in the cusp to various observed diamagnetic depression parameters: (d) difference between the minimum and maximum magnetic field, (e) minimum magnetic field, and (f) the average magnetic field. The Pearson correlation coefficient (r) is shown for both sets of data, with P_{RAM} and V having strong and moderate (respectively) positive correlations with ΔB , while the other comparisons show no correlation to each other.

pressures in the cusp to depress the field. However, we do not find this to be the case with our observations, and our results indicate that the dynamic pressure and the velocity in the solar wind are more important in creating the diamagnetic depressions.

The relevance of the He^{++} ions to the magnetic depression was also analyzed, and no strong correlation can be found between the number of helium counts and the depth of the depression, nor the minimum magnetic field nor the magnetic field strength in general. High He^{++} counts are observed for both low and high magnetic field depths. At Earth, it has been found that the depth of the magnetic field depression is strongly correlated to the energetic alpha particle counts [e.g., *Chen et al.*, 1998]. This shows that at Saturn (unlike at Earth), helium does not play a major role in depressing the local magnetic field.

All the summer cusp observations present magnetic field depression, with only two of the five cusp observations displaying depressions in the magnetic field in the winter hemisphere. At Earth it has been shown that magnetic field depressions are larger in the summer cusp [e.g., *Zhou et al.*, 2001]. This effect is due to the

summer cusp being tilted toward the incoming solar wind, where the magnetosheath flow is slower and the density is higher. This results in a plasma with a higher density entering the summer cusp and subsequently depressing the magnetic field more than for the case of the winter cusp. Therefore, if the magnetosheath flow is slower, and density is larger nearer the subsolar point, it would be expected that cusp magnetic field depressions should be stronger at lower latitudes relative to the planet-Sun line [Zhou *et al.*, 2001]. The magnetic field depressions at Saturn with respect to the latitudinal angle from the planet-Sun line are shown in Figure 9f, to see if there is a correlation. At Saturn the depth of the depressions are not observed to decrease with increasing latitude, so this argument is apparently not valid for Saturn.

6. Discussion

The magnetic depressions at Saturn cusp observations have been presented and characterized. A model of an axisymmetric internal magnetic field with a ring current field has been subtracted from the data. From this magnetic field subtraction, the magnetic pressure decrease in the depression was calculated and compared to observed plasma pressures, densities, and fluxes of the various plasma components.

Comparing to observations from depressions at Mercury [Winslow *et al.*, 2012], the magnetic pressure deficit from MESSENGER data shows much larger depths (tens of nanopascals) compared to the largest observed at Saturn (0.1 nPa). The observations are also more turbulent and short lived (minutes compared to hours). The superposed epoch analysis from the MESSENGER data of 169 cusp crossings (out of 279 orbits) shows that the magnetic depths are significantly larger. The depressions observed at Saturn are of the order of a few nanoteslas (the largest being ~ 10 nT for JAN07-b, with a background field of 15 nT), while at Mercury ~ 40 nT [Winslow *et al.*, 2012] with background fields of ~ 200 nT is typical (and large depressions of ~ 100 nT are observed with background fields of ~ 300 nT). The terrestrial cusp magnetic field does not fluctuate as much as at Mercury. Cusp depressions are more likely to be observed at Mercury and are more likely to be larger in magnitude due to the significantly larger solar wind dynamic pressure in the inner solar system.

From comparing the magnetic field and plasma measurements it has been shown that the particle and magnetic pressure changes do not compensate each other for most of the events. The method presented here calculates the magnetic pressure. From the figures showing the method (Figures 2, 4, 6, and 7), the model field magnitude is stronger than that measured by MAG. The model field can vary for different solar wind dynamic pressures and therefore magnetopause standoff distances, and without upstream monitors, this value can only be estimated. The polynomial addition removes any possibility of a larger background field that is caused by an unobservable global depression. This results in the calculated magnetic pressure deficit being a conservative lower estimate.

However, even with slightly more liberal calculations, the results would still not account for some of the large discrepancies with the plasma pressure observations. For most of the depressions, the CHEMS (usually the most dominant plasma pressure) pressure is 2 or 3 times larger than the magnetic pressure deficit, and for two examples they are lower. Also, for some observations the CHEMS pressure peaks do not match the troughs of the magnetic deficits. All the depressions in the cusp are observed during an increase (and a complete anticorrelation) in the low-energy electron density (where ELS is available), which is usually matched by a corresponding ELS pressure peak (but not necessarily a complete anticorrelation between magnetic and plasma pressure changes). This aspect is similar to the observations at the terrestrial cusp [Niehof *et al.*, 2008]. However, Niehof *et al.* [2008] found that the cusp diamagnetic cavities (CDCs) also occurred during increases in the energetic He^{++} counts, something that we do not always observe at Saturn's cusp. Unlike at Earth, we find no correlation of the energetic particle observation counts (He^{++}) to the depth of the diamagnetic depression.

This investigation introduces two different characteristic observations at Saturn, where although energetic He^{++} is observed in the depression, it is not always observed during the large low-energy electron density increases in the cusp, but instead in the adjacent magnetosphere. This was illustrated in Figures 4 and 5, where a higher-energy plasma population is observed in the magnetosphere, where the depression continues. This higher-energy electron population with slightly higher densities nearer the cusp is similar to terrestrial observations which were called the "cleft" in the 1980s, and once thought to be part of the cusp. An example of the terrestrial data (electrons with ions underneath) can be seen in Figure 10a [Newell and Meng, 1988]. The cusp region can be seen in the middle of the plot shown by the two white lines, followed by a boundary layer and then the cleft (the high-energy electrons and ions).

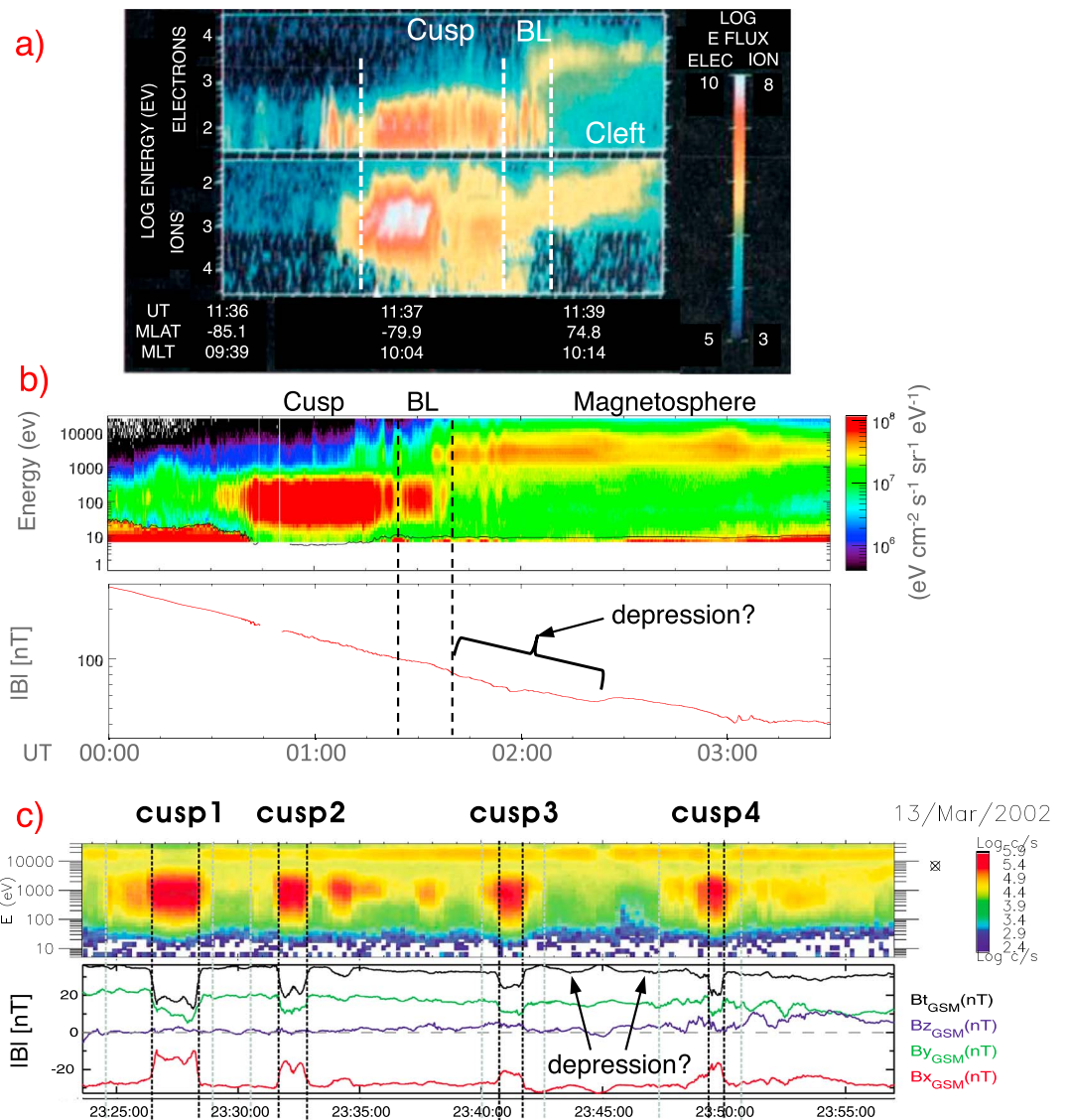


Figure 10. Earth observations of the cusp and magnetic field depressions. (a) Adapted from *Newell and Meng* [1988]; this panel shows a DMS-F7 cusp observation and the cleft region (later in time) with more energetic plasma. (b) Cluster (C2) electron data, where the spacecraft passes through the cusp and then (what is identified by *Bogdanova et al.* [2008]) the boundary layer BL, similar to the Saturn observations. The magnetic data also show a possible depression in the magnetosphere. (c) Adapted from *Shi et al.* [2009]; electron and magnetic data show the cusp and associated magnetic field depressions. Depressions are also observed in the adjacent magnetosphere.

A similar observation can be seen from the Cluster data (C2 spacecraft) in Figure 10b. This event was discussed (and the electron data presented) by *Bogdanova et al.* [2008]. The authors locate the boundary layer in many cusp crossings at midaltitudes of $\sim 6 R_E$ (which they identify to be a high-latitude extension of the low-latitude boundary layer), before entering the magnetosphere. The authors do not present the corresponding magnetometer data (shown here), which shows a possible depression in the adjacent magnetosphere. For terrestrial studies this would not be classed as a depression as it does not have a magnitude decrease of at least 20% [e.g., *Niehof et al.*, 2008, 2010]. This is very similar to the 8MAR07 observations, except that in the 8MAR07 interval, the depression occurs in both the cusp and the adjacent magnetosphere.

Other similar observations made by Cluster (C1) are presented in Figure 10c. Ion and magnetic data show multiple cusp observations with their corresponding magnetic depressions. However, in the adjacent region, where high-energy plasma is observed, a smaller depression is also observed (examples marked by the

labeled arrow in Figure 10c). These high-energy regions are labeled the “high-latitude-trapping region” by the authors [Shi *et al.*, 2009] and correspond to the last closed field lines of the magnetosphere.

The Saturn examples are slightly different, with the depressions not usually centered on the cusp as defined from the plasma observations. In the cusp the depression is usually anticorrelated with the low-energy plasma density and pressure. The particles producing a diamagnetic effect in the dense magnetosheath plasma depress the field in the cusp. As the spacecraft crosses out of the cusp, the larger plasma pressure continues to depress the magnetic field in the adjacent magnetospheric layer. This plasma pressure then decreases and the magnetic depression is no longer observed. But instead of causing two depressions like the previous Earth example, the depression is largely continuous.

Within this high-pressure plasma region in the magnetosphere, there are observations of increases in the He^{++} and water group (W^+) ion count, usually more so than in the cusp (except for the 1FEB07-b event). The composition of this plasma, as well as increases in the CHEMS pressure, shows that this is a mixed plasma. [Sergis *et al.*, 2013] showed that the magnetosheath has a presence of hot W^+ ; therefore, we do not know whether the observed W^+ is from the magnetosheath or directly from the magnetosphere.

If we assume that the He^{++} is observed due to an injection from the magnetosheath at the reconnection event, then we assume that the observed He^{++} is present on open field lines. Assuming this is the case, then an equatorward trajectory for a spacecraft (for the southern cusp observations), Cassini will have passed from the polar cap and then into the cusp filled with low-energy plasma (observed by CAPS) followed by further open field lines with the energetic particles (observed by CHEMS). This means that what we have assumed earlier is that the magnetosphere (and labeled as such in the plots) is actually an equatorward region of the cusp. Using a simple velocity filter paradigm observed in the cusp, this would make sense. Energetic particles have higher field-aligned velocities; therefore, they are observed more equatorward in the cusp than less energetic particles. However, this is not possible for the following reasons.

First, the ion energy-latitude dispersion observed in the IMS data would be expected to continue into this region. The plasma observations show the two regions to be more distinct from each other, with discrete boundaries. If this plasma is injected at the same time, there should not be a time separation (such as the one observed) between the observation of low-energy electrons and high-energy alpha particles. A 50 eV electron which is observed in the cusp by ELS would have an approximate field-aligned velocity of ~ 4000 km/s, while a 10 keV/ q He^{++} ion velocity would be ~ 1000 km/s. This would mean that the electrons should be observed closer to the open-closed field line boundary (i.e., more equatorward), but instead, the opposite is true.

If the field line is open, then the magnetospheric plasma would most likely have left the field line into the magnetosheath. A 1 keV equatorial magnetospheric electron at $L \sim 25$ (for the MAR07 example) would remain on a field line for ~ 3 min (assuming a near field-aligned equatorial pitch angle). The observation of the depression in the magnetosphere lasts approximately for 2 h (with He^{++} present). Since the magnetospheric plasma will only remain on an open field line for a few minutes, this field line cannot be newly opened as the spacecraft remains in this region for a significantly larger timescale. Furthermore, there is a boundary layer observed between the two regions that has been interpreted to be the high-latitude extension of the low-latitude boundary layer. An example of this can be seen in Figure 5 labeled BL. This layer separates the two regions and would not be expected to occur if this was one cusp observation (divided into two different energy layers).

Second, the observation of a significant increase in the water group ions upon entering the high-pressure plasma region where the depression continues provides evidence that these are closed field lines with magnetospheric plasma present. “Significant” here being defined by the fact that there are no W^+ ion counts observed above the detectability threshold of the instrument in the cusp, while they are detected in the high-pressure plasma region (in the magnetosphere). If these ions were from the magnetosheath, one would expect them to always be observed in the cusp simultaneously with the thermal plasma. This provides evidence that the labeling of this region “magnetosphere” remains correct but leaves the composition of the plasma unexplained. There must be a different mechanism that He^{++} enters the magnetosphere and is observed here, other than magnetic reconnection.

7. Conclusions

It has been shown that the magnetic depressions (mostly in the southern hemisphere) are not always centered on the cusp, but on the boundary with magnetospheric particles. The density of the plasma, which

is of magnetosheath origin, is anticorrelated to the magnetic field depression in the cusp. The high plasma pressure in the magnetosphere adjacent to the cusp acts to continue the depression of the magnetic field (into the magnetosphere). The presence of mixed plasma of solar wind and magnetospheric origin during the latter half of the depressions introduces a problem of exactly defining this layer. The layer could either be reconnected (open) field lines, with energized solar alpha particles, or the auroral current region which is observed to occur on the open-closed field line boundary. Due to the duration of the observation of this layer, this region is most likely to be on closed magnetospheric field lines, leaving the observation of solar wind particles an open question.

The plasma pressures in the cusp were sometimes found to overcompensate for the magnetic pressure decrease found in the depression. The combination of low depression depths found in the cusp at low magnetic field strengths (10–20 nT), and the absence of depressions in higher magnetic field strengths (30–40 nT) (unless there are very high electron densities) reveals the magnetic field to be much more difficult to depress at Saturn in comparison to observations at Earth and Mercury.

Highly energetic He⁺⁺ ions were observed during some portion of the magnetic depression in 7 out of 10 of the events. No significant correlation with the data available was found between the number of alpha particles observed and the depression of the magnetic field. This shows that although the helium ions are present, they are not necessarily the component of the plasma driving the depression in the observation at Saturn's cusp in comparison to Earth's.

The depressions are expected to be stronger in the summer hemisphere due to increased magnetosheath densities and lower velocities while entering the cusp at lower latitudes to the ecliptic (from Earth observations). A comparison of the latitudes of the depressions revealed no trend, and therefore, this expectation is inconclusive. Although most of the observations of the magnetic depressions at Saturn occur in the summer hemisphere, with only 10 data points, it is not possible to confirm this hypothesis with the limited observations from the Cassini spacecraft.

Acknowledgments

We thank the MSSL CAPS operations team, L. K. Gilbert, G. R. Lewis, and N. Shane, for support in calibration and data display. J.M.J. was supported by STFC Studentship ST/J500914/1 at MSSL-UCL. C.S.A. is supported by a Royal Society University Research Fellowship. M.F.T. was supported by the NASA Cassini Program through JPL contract 1243218 with Southwest Research Institute. We acknowledge support via the MSSL consolidated grant from STFC. All the data for this study can be found at NASA's planetary data system (<https://pds.jpl.nasa.gov>).

References

- Achilleos, N., C. S. Arridge, C. Bertucci, C. M. Jackman, M. K. Dougherty, K. K. Khurana, and C. T. Russell (2008), Large-scale dynamics of Saturn's magnetopause: Observations by Cassini, *J. of Geophys. Res.*, *113*, A11209, doi:10.1029/2008JA013265.
- Adamson, E., A. Otto, and K. Nykyri (2011), 3-D mesoscale MHD simulations of a cusp-like magnetic configuration: Method and first results, *Ann. Geophys.*, *29*(5), 759–770, doi:10.5194/angeo-29-759-2011.
- Adamson, E., A. Otto, and K. Nykyri (2012), 3-D mesoscale MHD simulations of magnetospheric cusp-like configurations: Cusp diamagnetic cavities and boundary structure, *Ann. Geophys.*, *30*(2), 325–341, doi:10.5194/angeo-30-325-2012.
- Asikainen, T., and K. Mursula (2005), Energetic particle fluxes in the exterior cusp and the high-latitude dayside magnetosphere: Statistical results from the Cluster/RAPID instrument, *Ann. Geophys.*, *23*(6), 2217–2230, doi:10.5194/angeo-23-2217-2005.
- Arridge, C. S., L. K. Gilbert, G. R. Lewis, E. C. Sittler, G. H. Jones, D. O. Kataria, A. J. Coates, and D. T. Young (2009), The effect of spacecraft radiation sources on electron moments from the Cassini CAPS electron spectrometer, *Planet. Space Sci.*, *57*(7), 854–869, doi:10.1016/j.pss.2009.02.011.
- Arridge, C. S., et al. (2016), Cassini observations of Saturn's southern polar cusp, *J. Geophys. Res. Space Physics*, *121*, 3006–3030, doi:10.1002/2015JA021957.
- Bogdanova, Y. V., et al. (2008), Formation of the low-latitude boundary layer and cusp under the northward IMF: Simultaneous observations by Cluster and Double Star, *J. Geophys. Res.*, *113*, A07507, doi:10.1029/2007JA012762.
- Bunce, E. J., S. W. H. Cowley, I. I. Alexeev, C. S. Arridge, M. K. Dougherty, J. D. Nichols, and C. T. Russell (2007), Cassini observations of the variation of Saturn's ring current parameters with system size, *J. Geophys. Res.*, *112*, A10202, doi:10.1029/2007JA012275.
- Burton, M. E., M. K. Dougherty, and C. T. Russell (2010), Saturn's internal planetary magnetic field, *Geophys. Res. Lett.*, *37*, L24105, doi:10.1029/2010GL045148.
- Cargill, P. J., et al. (2005), Cluster at the magnetospheric cusps, *Space Sci. Rev.*, *118*, 321–366, doi:10.1007/s11214-005-3835-0.
- Chen, J., and T. A. Fritz (1998), Correlation of cusp MeV helium with turbulent ULF power spectra and its implications, *Geophys. Res. Lett.*, *25*(22), 4113–4116, doi:10.1029/1998GL900122.
- Chen, J., T. A. Fritz, R. B. Sheldon, H. E. Spence, W. N. Spjeldvik, J. F. Fennell, and S. Livi (1997), A new, temporarily confined population in the polar cap during the August 27, 1996 geomagnetic field distortion period, *Geophys. Res. Lett.*, *24*, 1447–1450, doi:10.1029/97GL01369.
- Chen, J., et al. (1998), Cusp energetic particle events: Implications for a major acceleration region of the magnetosphere, *J. Geophys. Res.*, *103*, 69–78, doi:10.1029/97JA02246.
- Connerney, J. E. P., M. H. Acuna, and N. F. Ness (1981), Modeling the Jovian current sheet and inner magnetosphere, *J. Geophys. Res.*, *86*, 8370–8384, doi:10.1029/JA086iA10p08370.
- Connerney, J. E. P., M. H. Acuna, and N. F. Ness (1983), Currents in Saturn's magnetosphere, *J. Geophys. Res.*, *88*, 8779–8789, doi:10.1029/JA088iA11p08779.
- Cui, J., R. V. Yelle, and K. Volk (2008), Distribution and escape of molecular hydrogen in Titan's thermosphere and exosphere, *J. Geophys. Res.*, *113*, E10004, doi:10.1029/2007JE003032.
- Delcourt, D. C., and J.-A. Sauvaud (1999), Populating of the cusp and boundary layers by energetic (hundreds of keV) equatorial particles, *J. Geophys. Res.*, *104*(A10), 22,635–22,648, doi:10.1029/1999JA900251.
- Dougherty, M. K., et al. (2004), The Cassini magnetic field investigation, *Space Sci. Rev.*, *114*, 331–383, doi:10.1007/s11214-004-1432-2.
- Eastman, T. E., S. A. Boardsen, S.-H. Chen, S. F. Fung, and R. L. Kessel (2000), Configuration of high-latitude and high-altitude boundary layers, *J. Geophys. Res.*, *105*, 23,221–23,238, doi:10.1029/1999JA900269.

- Erlanson, R. E., L. J. Zanetti, T. A. Potemra, M. Andre, and L. Matson (1988), Observation of electromagnetic ion cyclotron waves and hot plasma in the polar cusp, *Geophys. Res. Lett.*, *15*, 421–424, doi:10.1029/GL015i005p00421.
- Frank, L. A. (1971), Plasma in the Earth's polar magnetosphere, *J. Geophys. Res.*, *76*, 5202–5219, doi:10.1029/JA076i022p05202.
- Fritz, T. A., J. Chen, and G. L. Siscoe (2003), Energetic ions, large diamagnetic cavities, and Chapman-Ferraro cusp, *J. Geophys. Res.*, *108*, 1028, doi:10.1029/2002JA009476.
- Giampieri, G., and M. Dougherty (2004), Modelling of the ring current in Saturn's magnetosphere, *Ann. Geophys.*, *22*, 653–659, doi:10.5194/angeo-22-653-2004.
- Jackman, C. M., N. Achilleos, E. J. Bunce, S. W. H. Cowley, M. K. Dougherty, G. H. Jones, S. E. Milan, and E. J. Smith (2004), Interplanetary magnetic field at ~ 9 AU during the declining phase of the solar cycle and its implications for Saturn's magnetospheric dynamics, *J. Geophys. Res.*, *109*, A11203, doi:10.1029/2004JA010614.
- Jasinski, J. M., et al. (2014), Cusp observation at Saturn's high-latitude magnetosphere by the Cassini spacecraft, *Geophys. Res. Lett.*, *41*, 1382–1388, doi:10.1002/2014GL059319.
- Jasinski, J. M., C. S. Arridge, A. J. Coates, G. H. Jones, N. Sergis, M. F. Thomsen, D. B. Reisenfeld, N. Krupp, and J. H. Waite (2016a), Cassini plasma observations of Saturn's magnetospheric cusp, *J. Geophys. Res. Space Physics*, *121*, 12,047–12,067, doi:10.1002/2016JA023310.
- Jasinski, J. M., J. A. Slavin, C. S. Arridge, G. Poh, X. Jia, N. Sergis, A. J. Coates, G. H. Jones, and J. H. Waite (2016b), Flux transfer event observation at Saturn's dayside magnetopause by the Cassini spacecraft, *Geophys. Res. Lett.*, *43*, 6713–6723, doi:10.1002/2016GL069260.
- Kellett, S., C. S. Arridge, E. J. Bunce, A. J. Coates, S. W. H. Cowley, M. K. Dougherty, A. M. Persoon, N. Sergis, and R. J. Wilson (2010), Nature of the ring current in Saturn's dayside magnetosphere, *J. Geophys. Res.*, *115*, A08201, doi:10.1029/2009JA015146.
- Korth, H., et al. (2011), Plasma pressure in Mercury's equatorial magnetosphere derived from MESSENGER Magnetometer observations, *Geophys. Res. Lett.*, *38*, L22201, doi:10.1029/2011GL049451.
- Krimigis, S. M., et al. (2004), Magnetosphere imaging instrument (MIMI) on the Cassini mission to Saturn/Titan, *Space Sci. Rev.*, *114*, 233–329, doi:10.1007/s11214-004-1410-8.
- Lavraud, B., A. Fedorov, E. Budnik, A. Grigoriev, P. J. Cargill, M. W. Dunlop, H. Rème, I. Dandouras, and A. Balogh (2004), Cluster survey of the high-altitude cusp properties: A three-year statistical study, *Ann. Geophys.*, *22*(8), 3009–3019, doi:10.5194/angeo-22-3009-2004.
- Linder, D. R., A. J. Coates, R. D. Woodliffe, C. Alsop, A. D. Johnstone, M. Grande, A. Preece, B. Narheim, and D. T. Young (1998), The Cassini CAPS electron spectrometer, in *Measurement Techniques for Space Plasmas: Particles*, vol. 102, edited by R. E. Pfaff, J. E. Borovsky, and D. T. Young, p. 257, AGU, Washington, D. C.
- Lockwood, M., T. G. Onsager, C. J. Davis, M. F. Smith, and W. F. Denig (1994), The characteristic of the magnetopause reconnection X-line deduced from low-altitude satellite observations of cusp ions, *Geophys. Res. Lett.*, *21*, 2757–2760, doi:10.1029/94GL02696.
- Newell, P. T., and C.-I. Meng (1988), The cusp and the cleft/boundary layer—Low-altitude identification and statistical local time variation, *J. Geophys. Res.*, *93*, 14,549–14,556, doi:10.1029/JA093iA12p14549.
- Nichols, J. D., J. T. Clarke, S. W. H. Cowley, J. Duval, A. J. Farmer, J.-C. Gérard, D. Grodent, and S. Wannawichian (2008), Oscillation of Saturn's southern auroral oval, *J. Geophys. Res.*, *113*, A11205, doi:10.1029/2008JA013444.
- Niehof, J. T., T. A. Fritz, R. H. W. Friedel, and J. Chen (2008), Interdependence of magnetic field and plasma pressures in cusp diamagnetic cavities, *Geophys. Res. Lett.*, *35*, L11101, doi:10.1029/2008GL033589.
- Niehof, J. T., T. A. Fritz, R. H. W. Friedel, and J. Chen (2010), Size and location of cusp diamagnetic cavities observed by Polar, *J. Geophys. Res.*, *115*, A07201, doi:10.1029/2009JA014827.
- Nykyri, K., A. Otto, E. Adamson, and A. Tjulin (2011a), On the origin of fluctuations in the cusp diamagnetic cavity, *J. Geophys. Res.*, *116*, A06208, doi:10.1029/2010JA015888.
- Nykyri, K., A. Otto, E. Adamson, E. Dougal, and J. Mumme (2011b), Cluster observations of a cusp diamagnetic cavity: Structure, size, and dynamics, *J. Geophys. Res.*, *116*, A03228, doi:10.1029/2010JA015897.
- Nykyri, K., A. Otto, E. Adamson, E. Kronberg, and P. Daly (2012), On the origin of high-energy particles in the cusp diamagnetic cavity, *87–88*, 70–81, doi:10.1016/j.jastp.2011.08.012, physical Process in the Cusp: Plasma Transport and Energization.
- Pitout, F., C. P. Escoubet, B. Klecker, and I. Dandouras (2009), Cluster survey of the mid-altitude cusp—Part 2: Large-scale morphology, *Ann. Geophys.*, *27*, 1875–1886, doi:10.5194/angeo-27-1875-2009.
- Poh, G., et al. (2016), Messenger observations of cusp plasma filaments at Mercury, *J. Geophys. Res. Space Physics*, *121*, 8260–8285, doi:10.1002/2016JA022552.
- Raines, J. M., D. J. Gershman, J. A. Slavin, T. H. Zurbuchen, H. Korth, B. J. Anderson, and S. C. Solomon (2014), Structure and dynamics of Mercury's magnetospheric cusp: Messenger measurements of protons and planetary ions, *J. Geophys. Res. Space Physics*, *119*, 6587–6602, doi:10.1002/2014JA020120.
- Sergis, N., S. M. Krimigis, D. G. Mitchell, D. C. Hamilton, N. Krupp, B. H. Mauk, E. C. Roelof, and M. K. Dougherty (2009), Energetic particle pressure in Saturn's magnetosphere measured with the magnetospheric imaging instrument on Cassini, *J. Geophys. Res.*, *114*, A02214, doi:10.1029/2008JA013774.
- Sergis, N., et al. (2010), Particle pressure, inertial force, and ring current density profiles in the magnetosphere of Saturn, based on Cassini measurements, *Geophys. Res. Lett.*, *37*, L02102, doi:10.1029/2009GL041920.
- Sergis, N., C. M. Jackman, A. Masters, S. M. Krimigis, M. F. Thomsen, D. C. Hamilton, D. G. Mitchell, M. K. Dougherty, and A. J. Coates (2013), Particle and magnetic field properties of the Saturnian magnetosheath: Presence and upstream escape of hot magnetospheric plasma, *J. Geophys. Res. Space Physics*, *118*, 1620–1634, doi:10.1002/jgra.50164.
- Sergis, N., C. M. Jackman, M. F. Thomsen, S. M. Krimigis, D. G. Mitchell, D. C. Hamilton, M. K. Dougherty, N. Krupp, and R. J. Wilson (2017), Radial and local time structure of the Saturnian ring current, revealed by Cassini, *J. Geophys. Res. Space Physics*, *122*, 1803–1815, doi:10.1002/2016JA023742.
- Shi, Q. Q., et al. (2009), Cluster observations of the entry layer equatorward of the cusp under northward interplanetary magnetic field, *J. Geophys. Res.*, *114*, A12219, doi:10.1029/2009JA014475.
- Slavin, J. A., et al. (2014), MESSENGER observations of Mercury's dayside magnetosphere under extreme solar wind conditions, *J. Geophys. Res. Space Physics*, *119*, 8087–8116, doi:10.1002/2014JA020319.
- Smith, M. F., and M. Lockwood (1996), Earth's magnetospheric cusps, *Rev. Geophys.*, *34*, 233–260, doi:10.1029/96RG00893.
- Thomsen, M. F., D. B. Reisenfeld, D. M. Delapp, R. L. Tokar, D. T. Young, F. J. Crary, E. C. Sittler, M. A. McGraw, and J. D. Williams (2010), Survey of ion plasma parameters in Saturn's magnetosphere, *J. Geophys. Res.*, *115*, A10220, doi:10.1029/2010JA015267.
- Trattner, K. J., S. A. Fuselier, W. K. Peterson, and S.-W. Chang (1999), Comment on "Correlation of cusp MeV helium with turbulent ULF power spectra and its implications", *Geophys. Res. Lett.*, *26*, 1361–1362, doi:10.1029/1999GL900284.
- Trattner, K. J., S. A. Fuselier, W. K. Peterson, S.-W. Chang, R. Friedel, and M. R. Aellig (2001), Origins of energetic ions in the cusp, *J. Geophys. Res.*, *106*, 5967–5976, doi:10.1029/2000JA003005.

- Trattner, K. J., S. A. Fuselier, W. K. Peterson, S.-W. Chang, R. Friedel, and M. R. Aellig (2003), Reply to comment on "Origins of energetic ions in the cusp" by R. Sheldon, J. Chen, and T. A. Fritz, *J. Geophys. Res.*, *108*, 1303, doi:10.1029/2002JA009781.
- Trattner, K. J., S. M. Petrinec, S. A. Fuselier, K. Nykyri, and E. Kronberg (2011), Cluster observations of bow shock energetic ion transport through the magnetosheath into the cusp, *J. Geophys. Res.*, *116*, A09207, doi:10.1029/2011JA016617.
- Tsyganenko, N. A., and C. T. Russell (1999), Magnetic signatures of the distant polar cusps: Observations by polar and quantitative modeling, *J. Geophys. Res.*, *104*, 24,939–24,956, doi:10.1029/1999JA900279.
- Winslow, R. M., C. L. Johnson, B. J. Anderson, H. Korth, J. A. Slavin, M. E. Purucker, and S. C. Solomon (2012), Observations of Mercury's northern cusp region with MESSENGER's Magnetometer, *Geophys. Res. Lett.*, *39*, L08112, doi:10.1029/2012GL051472.
- Young, D. T., et al. (2004), Cassini plasma spectrometer investigation, *Space Sci. Rev.*, *114*, 1–112, doi:10.1007/s11214-004-1406-4.
- Zhou, X. W., C. T. Russell, G. Le, S. A. Fuselier, and J. D. Scudder (2000), Solar wind control of the polar cusp at high altitude, *J. Geophys. Res.*, *105*, 245–252, doi:10.1029/1999JA900412.
- Zhou, X. W., C. T. Russell, G. Le, S. A. Fuselier, and J. D. Scudder (2001), Factors controlling the diamagnetic pressure in the polar cusp, *Geophys. Res. Lett.*, *28*, 915–918, doi:10.1029/2000GL012306.
- Zieger, B., and K. C. Hansen (2008), Statistical validation of a solar wind propagation model from 1 to 10 AU, *J. Geophys. Res.*, *113*, A08107, doi:10.1029/2008JA013046.